Highly active composite TiO2-polypyrrole nanostructures for water and air depollution under visible light irradiation

Xiaojiao Yuan, Marek Kobylanski, Zhenpeng Cui, Jian Li, Patricia Beaunier, Diana Dragoe, Christophe Colbeau-Justin, Adriana Zaleska-Medynska, Hynd Remita

Highly Active Composite TiO_2-Polypyrrole Nanostructures for Water and Air Depollution Under Visible Light Irradiation

Xiaojiao Yuan[1], Marek P. Kobylanski[2], Zhenpeng Cui[1], Jian Li[1], Patricia Beaunier[3], Diana Dragoe[4], Christophe Colbeau-Justin[1], Adriana Zaleska-Medynska[2], Hynd Remita[1,5*]

[1] Institut de Chimie Physique, UMR 8000 CNRS, Université Paris-Saclay, 91405 Orsay, France

[2] Department of Environmental Technology, Faculty of Chemistry, University of Gdansk, 80-308 Gdansk, Poland

[3] Sorbonne Université, CNRS, UMR 7197, Laboratoire de Réactivité de Surface, 75005 Paris, France

[4] Institut de Chimie Moléculaire et des Matériaux d'Orsay, Université Paris-Saclay, 91405 Orsay, France

[5] CNRS, Institut de Chimie Physique, UMR 8000, 91405 Orsay, France

E-mail : hynd.remita@universite-paris-saclay.fr

Abstract

Engineering photocatalytic materials for solar energy harvesting and environmental remediation is a very promising prospect to solve energy and environment issues. Here we report the preparation of a nanocomposite formed by TiO_2 with nanostructured polypyrrole (PPy_{NS}-TiO_2) and its photocatalytic properties. We show that this nanocomposite is very active for water and air treatment under UV and visible light irradiation. This activity is higher than that of bare TiO_2 and PPy_{NS}, and much improved compared to that of TiO_2-bulk polypyrrole (PPy_{bulk}-TiO_2). The nanostructuration of the conjugated

polymer is a key factor for the photocatalytic activity of the composite. The large enhancement of the photocatalytic activity is ascribed to the heterojunction between PPy_{NS} and TiO_2, which broadens the absorption of visible light and facilitates the charge carriers' separation. These results foresee the composite PPy_{NS}-TiO_2 photocatalyst for water and air purification in environment remediation.

Keywords: Polypyrrole nanostructures, Organic-inorganic hybrid nanocomposites, Conjugated polymers, Titanium dioxide, Photocatalysis, Depollution.

1. Introduction

Semiconductor photocatalysts based on TiO_2 have attracted increasing attention for water and air treatment owing to the low cost of titania, its high photochemical properties, excellent stability and outstanding photocatalytic activity [1-6]. Nevertheless, the large band gap of TiO_2 (3.2 eV for anatase and 3.0 eV for rutile) induces a photocatalytic activity only under ultraviolet light (5% of the solar light), which limits its commercial applications in photocatalysis. Besides, high charge carrier recombination in TiO_2 also results in a poor photocatalytic activity. In order to improve its photocatalytic activity, numerous approaches have been developed such as noble metal loading [7-13], non-metal doping [14-16], heterojunction construction [4, 13, 17-19] or modification with conjugated polymers (CPs) [20-27]. Organic-inorganic hybrid materials have attracted much attention in solar energy conversion and photocatalytic degradation of organic pollutants [28, 29]. Among them, modification of TiO_2 with conjugated polymer nanostructures (CPNs) presents promising photocatalysis application under visible light. CPs with their unique extending π-π^* electron system which can serve as stable photosensitizers inpouring the electrons into the conduction band (CB) of semiconductors [26, 30-33]. For example, composite materials composed of TiO_2 nanoparticles bound to large PPy polymer particles surface were reported to be photoactive under visible-light irradiation [27]. Although there are already some investigations on photocatalytic performance of TiO_2-PPy, some fundamental questions are still not answered. In previous studies, little attention was paid to the life time of photo-induced charge carriers and charge transfer route between TiO_2 and PPy nanostructures under ultraviolet and visible light, separately and the photocatalytic properties of TiO_2-PPy nanocomposite for air treatment has not been reported [20, 22, 23, 27, 34].

CPs present high mobility of charge carriers, narrow and tunable band gap, good stability and high absorption coefficients towards the visible region or near-infrared light. These excellent and special properties indicate that CPs are promising photosensitizers or photocatalysts under the solar light illumination. We demonstrated in our previous works that nanostructured CPs such as poly(diphenylbutadyine) PDPB, Poly(3,4-ethylenedioxythiophene) PDOT, Poly(3-hexylthiophene) (P3HT) and polypyrrole (PPy), exhibit higher photocatalytic property in visible region contrary to their bulk counterpart, and this activity is much higher than that of plasmonic TiO_2 [31, 33, 35]. These CPNs are synthesized in soft templates formed by hexagonal or lamellar mesophases and polymerized by UV light or radiolysis [30, 36, 37].

In this work, we modified commercial P25 TiO_2 with nanostructured PPy (PPy_{NS}) (prepared in soft templates formed by hexagonal mesophases) for photodegradation of organic pollutants (methyl orange and phenol as model water pollutants and toluene as air pollutant). The nanocomposite shows an important increase of the photocatalytic performance under ultraviolet and visible light compared to bare TiO_2 and $PPy_{NS,}$ and most interestingly to PPy_{bulk}-TiO_2. The improved photocatalytic performance of PPy_{NS}-TiO_2 is due to highest surface area and less defects in the nanostructure PPy and to the wide light absorption and increased charge separation efficiency owing to the heterojunction formation. The PPy_{NS}-TiO_2 composite photocatalyst shows high stability and recyclability. The kinetics of charge carriers is also discussed. This work offers a facile and cheap way to fabricate the heterojunction in organic-inorganic hybrid materials interface, and the composite nanomaterial represents a promising photocatalyst for water treatment and indoor application such as air treatment.

2. Experimental

2.1 Chemicals and materials

Pyrrole (Py) (98%), iron chloride ($FeCl_3$, ≥97%), sodium dodecyl sulfate (SDS, 98.5%), cyclohexane (99.7%), n-pentanol (>99%), methyl orange (MO), phenol, sodium chloride (NaCl, ≥99.5%), ethanol (≥ 99%), were bought from Aldrich Chemical Co., and toluene was purchased P.P.H. "STANLAB" (Lublin, Poland). All the reagents were used without further purification. Commercial P25 titanium dioxide purchased from EVONIK has been used as support material, which consists of crystalline phases rutile (14-17%), anatase (73-85%) and amorphous titania (0-13%) [38]. Distilled water was used throughout the experiment.

2.2 Photocatalyst preparation

PPy nanostructures (PPy_{NS}) were obtained by surfactant-mediated soft templating (lamellar mesophases) method: We used the synthetic protocol reported in our previous work with some modifications [31]. In short, first, the monomer pyrrole (100 µL) and 1.6 mg of the SDS surfactant were dissolved in 4 mL aqueous NaCl (0.1 M). Then 6 mL cyclohexane and 1 mL pentanol were then added to the solution, the obtained mesophase doped by monomer was labeled as A. The mesophase B was prepared: An aqueous solution (4 mL) containing 0.1 M $FeCl_3$ and SDS surfactant (1.6 mg) was added under stirring to cyclohexane (6 mL) and pentanol (1 mL). The achieved mixture (A+B) was vigorously stirred with vortex, and kept 12 h for complete polymerization. The polymerization takes place in the confined aqueous domain. The PPy nanostructures powder was extracted with a mixture ethanol and distilled water.

The composite PPy_{NS}-TiO_2 was obtained by sonication (5 min) in ethanol followed by 2 h stirring

(**Fig. S1a**). PPy_{bulk} was synthesized without any soft template (polymerization in water using $FeCl_3$ as oxidant) [31]. PPy_{bulk}-TiO_2 was prepared with the sample procedure used for PPy_{NS}-TiO_2 preparation.

Modification of TiO_2 with Ag NPs (Ag-TiO_2) was obtained by radiolytic reduction (using a panoramic gamma source) of Ag^+ on TiO_2 in suspension in water (containing 0.1 M of 2-propanol as $HO^{\cdot}$ scavenger) as reported in our previous work [10, 12]. Here, Ag-TiO_2 plasmonic photocatalyst is taken as a model photocatalyst to be compared with PPy_{NS}-TiO_2 due to its good photocatalytic activity under visible light.

2.3. Characterization

UV-visible spectra of PPy_{NS}-TiO_2, PPy_{NS} and TiO_2 were recorded with a Cary 5000 Series, Agilent Technologies spectrophotometer using an integrating sphere and with KBr as a reference sample. The morphology of the synthesized materials was observed by transmission electron microscopy (TEM, JEOL JEM 2010 UHR operating at 200 kV).

The crystalline structure of the samples was studied using an X-ray diffraction (XRD) (PHILIPS-PW 3040/60) system with Cu Kα radiation from 10~90º.

FT-IR (Fourier transform infrared) spectra were recorded using a FT-IR spectrometer (Bruker Vertex 70) with a diamond/ZnSe accessory (PIKEMIRACLE crystal plate) and a dectector LN-MCT Mid equipped with a cooling system (liquid nitrogen).

X-ray photospectroscopy (XPS) surveys were conducted on a Kα X-ray Photoelectron Spectrometer equipped with a hemispherical electron energy analyzer (Mg Kα radiation and monochromatic Al Kα, PHI 5000 VersaProbe II microprobe) under ultrahigh vacuum. For charge

correction, C1 spectra at 284.5 eV as standard was considered. The samples were dispersed in ethanol and then supported on Si plate for measurements.

Time-resolved microwave conductivity (TRMC) technique was used to investigate the photogenerated charge carriers' dynamics of the as-prepared samples under UV and visible light excitation. A pulsed and tunable laser source (200 ~ 2000 nm) equipped with an optical parametric oscillator (OPO; EKSPLA, NT342B) was used to excite the samples and a Gunn diode (30 GHz) was used to generate microwaves. TRMC technique measures the relative change ($\frac{\Delta P(t)}{p}$) in microwave power reflected from a semiconductor material during its excitation by a laser pulse. This change ($\Delta\sigma(t)$) could be related to small perturbation of the samples conductivity, as shown in the following formula:

$$\frac{\Delta P(t)}{p} = A\Delta\sigma(t) = Ae\mu_e\Delta n_e(t) \quad \text{(equation 1)}$$

In TiO_2 based compounds, the electron mobility (μ_e) is much higher than of h^+. Therefore, $\Delta\sigma(t)$ is mainly due to excess electrons. $\Delta n_e(t)$ is the excess free electron number at time t. A (sensitivity factor) is time independent and relies on the conductivity of the semiconductor and the microwave frequency.

The primary data given by TRMC signals are its maximum value (I_{max}), which corresponds the quantity of the excess electrons generated by the laser pulse, and its decay, which is owing to the decrease of excess electrons.

The photoelectrochemical performance of the as-prepared samples were measured by Origalys workstation with a three-electrode system (the prepared sample electrode, Pt foil electrode and Ag/AgCl electrode were acted as working, counter and reference electrode, respectively). The

photoinduced current density with time (*i-t)* curves were observed at a potential of -200 V (*vs.* Ag/AgCl). The electrochemical impedance spectroscope (EIS) measurements were conducted in 0.1 M Na_2SO_4 solution. The working electrodes were prepared by a highly homogeneous sample film on FTO substrate. In briefly, 3 mg of sample was dispersed in 3 mL ethanol by stirring. Then, the solution was spread on the FTO (fluorine doped tin oxide) substrate. Finally, the working electrodes were achieved after they were dried at room temperature. EIS was recorded with AC voltage amplitude of 10 mV, and a frequency range from 0.1 Hz to 1000 Hz at 0.2 V (*vs*. Ag/AgCl).

2.4. Photoactivity tests

The photocatalytic property of PPy_{NS}-TiO_2 was investigated for degradation of methyl orange (MO, 500 ppm) and phenol (C_6H_5OH, 50 ppm) in water and toluene (C_7H_8, 200 ppm) in air.

Phenol is one of the most commonly used test molecule. It was proposed by Serpone et al. as a standard test molecule, it shows some advantages [39]:

- It does not degrade by photolysis or catalysis.
- It has an absorption band at 269 nm and can be detected by UV-visible spectroscopy.
- Its mechanism of degradation is known (the main intermediates being benzoquinone, hydroquinone and catechol) [40].
- It can be completely mineralized into CO_2 and H_2O.
- Its adsorption on the surface of TiO_2 is very weak.
- It is a real pollutant of water.

Methyl orange is a toxic azo-dye used in textile industry.

Before irradiation, 3 mg of the photocatalyst (PPy_{NS}-TiO_2, bare PPy_{NS}, TiO_2 or PPy_{bulk}-TiO_2) was dispersed in 3 mL of water containing phenol (initial concentration C_0 = 50 ppm) or MO (initial concentration C_0 = 500 ppm) used as model organic pollutant. In order to ensure adsorption-desorption equilibrium, the mixture was stirred for 2 h in the dark. Control tests for photolysis (without photocataysts) were conducted under UV light **(Fig. S2)**. Then, the samples were exposed to a UV-visible light (Oriel 300 W Xenon lamp) or a visible light (Oriel 300 W Xenon lamp with a 420-nm cut off filter) under O_2 bubbling. 400 µL of the mixture were taken out every 5 min under UV irradiation and 1 h under visible light, respectively. Then, the suspension was centrifuged to separate the catalyst from the solution. High pressure liquid chromatography (HPLC, Agilent Technologies 1260 Infinity) was used to measure the concentration of phenol. The calibration of phenol was shown in **Fig. S3**. And the concentration of MO was determined by UV-vis spectrophotometric method. The photocatalytic activity of the sample was estimated by the expression $(C_0\text{-}C)/C_0 \times 100\%$ (C_0: initial concentration; C: present concentration after every interval of time).

To estimate the quantity of the mineralized pollutant, we used Total organic carbon (TOC) (Shimadzu TOC-LCSH).

Toluene was used as an air pollutant model. The photocatalytic tests in gas phase were conducted in a gas reactor with the volume of 30 cm^3. The reactor for photodegradation of gas is equipped with the LED diodes, which emit monochromatic irradiation (375 nm, 415 nm or 465 nm). The light intensity of the irradiation corresponded to 10 mW/cm^2. A slide of glass (2 cm × 2 cm) was covered by PPy_{NS}, TiO_2, and PPy_{NS}-TiO_2 film, respectively, and then the samples were placed on the bottom of the reactor and sealed with a quartz window (**Fig. S1d**). The initial toluene concentration was 200

ppm. For UV and visible irradiation, we used LED arrays with λ = 375 nm, 415 nm and 465 nm. Before illumination, the reactor was kept in the dark for 10 min. To analyze the concentration of toluene by gas chromatography we used a GC, Clarus 500, PerkinElmer.

3. Results and discussions

3.1. Characterizations of PPy_{NS}-TiO_2 composite

The optical absorption properties of bare TiO_2 and PPy_{NS}, and PPy_{NS}-TiO_2 composite were investigated by UV-Vis DRS. In **Fig. 1a**, TiO_2 presents an absorption edge at 400 nm owing to the appearance of rutile, while the absorption edge of PPy_{NS}-TiO_2 is located at 490 nm. The composite PPy_{NS}-TiO_2 shows higher absorption in the visible range because of the interaction between PPy_{NS} and TiO_2 in heterojunction leading to a red shift of the absorbance towards the visible region. **Fig. S4** shows a broad absorption of PPy_{NS} from 200 nm to 800 nm. The optical band gap (E_g) of photocatalysts samples can be evaluated by DRS spectra (Kubelka-Munk method). The E_g of PPy_{NS}-TiO_2 and TiO_2 are 1.95 eV and 2.93 eV, respectively, which could be calculated by the plots of $(\alpha h\nu)^{1/2}$ *vs* $h\nu$ (α – absorption coefficient; h – Planck constant; ν – light frequency) (**Fig. 1b**)[41]. The band gap of PPy_{NS} is about 2.01 eV, which was calculated in our previous work [31]. **Fig. 1** and **Fig. S5** show broader light absorption and narrower band gap of PPy_{NS}-TiO_2 and PPy_{bulk}-TiO_2 compared with unmodified TiO_2. The broad absorption in visible light and narrow band gap (Eg < 3.2 eV) of catalyst are beneficial for photocatalytic activity under visible light.

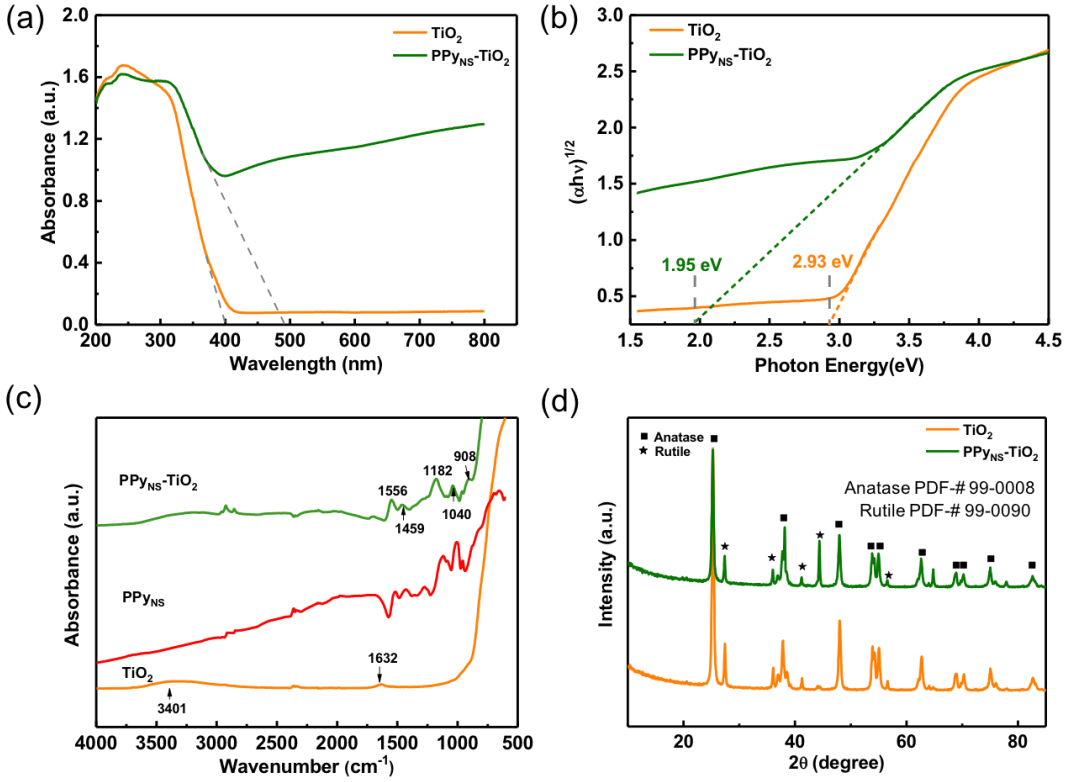

Fig. 1. (a) DRS spectra of composite PPy$_{NS}$-TiO$_2$ and bare TiO$_2$; (b) Kubelka-Munk plots and band energy estimation of PPy$_{NS}$-TiO$_2$ and TiO$_2$; (c) FTIR spectra of TiO$_2$, PPy$_{NS}$ and PPy$_{NS}$-TiO$_2$; (d) X-ray diffraction pattern for TiO$_2$ and PPy$_{NS}$-TiO$_2$.

FTIR is used to analyze the chemical structures of the as-prepared samples. The typical characteristic spectrum of PPy$_{NS}$-TiO$_2$ composite within the wavenumber range of 500 cm^{-1} ~ 4000 cm^{-1} is shown in **Fig. 1c**. The bands at 1556 cm^{-1} and 1459 cm^{-1} are assigned to the C=C and C-C stretching vibration of pyrrole ring, respectively. The peaks at 1182 cm^{-1} and 1040 cm^{-1} relate to the N-C stretching band and =C-H in-plane deformation vibration [42, 43]. The peak at 908 cm^{-1} is due to C-H out-of-plane bending vibrations [22]. The wide absorption peak at 500 cm^{-1} to 800 cm^{-1} refers to the flexural vibration of Ti-O-Ti in TiO$_2$, and the weak peak at 1632 cm^{-1} is vibration of O-H in water adsorbed on TiO$_2$ surface [44]. The broad peak at 3401 cm^{-1} is ascribed to the O-H vibration of

water molecular. The characteristic peaks of PPy_{NS}-TiO_2 composite are shifted compared to neat PPy_{NS} and TiO_2 indicating the interaction between PPy_{NS} and TiO_2.

Fig. 1d presents the XRD patterns of photocatalysts. For pristine TiO_2, the XRD patterns presents the characteristic diffraction peaks of both rutile and anatase and. The PPy_{NS}-TiO_2 composite shows similar diffraction patterns with TiO_2, and no other peaks were observed, which reveals the high purity of the sample.

TEM and SEM images of TiO_2 and PPy nanostructures and PPy_{NS}-TiO_2 composite are shown in **Fig. 2** and **Fig. S1b-c**, respectively. TiO_2-P25 particles show irregular shapes with diameters of 5-10 nm (**Fig. 2a and Fig. S6**), and the lattice spacing d = 0.25 nm of TiO_2 correspond to the (101) planes of rutile phase. PPy_{NS} are homogeneous in size (about 40 nm diameter) (**Fig.2b and Fig. S1b**) [31]. PPy_{NS}-TiO_2 composite exhibits higher contrast than amorphous organic PPy nanostructures (TiO_2 nanoparticles appear more dark) (**Fig. 2c-d** and **Fig. S1c**).

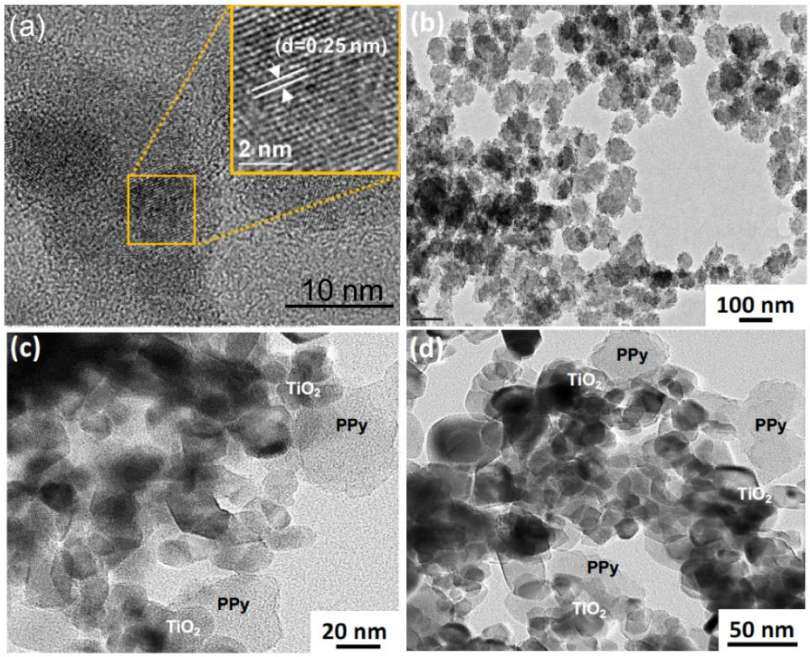

Fig. 2. HRTEM images of TiO_2 with the inter-planar distance corresponding to the (101) planes of rutile phase in inset (a); TEM images of PPy_{NS} (b) and PPy_{NS}-TiO_2 (c-d).

XPS was utilized to characterize the surface chemical components of PPy_{NS}-TiO_2 composite (**Fig. S7 and Fig.3**). The XPS survey spectra presents the elements of Ti, O, C, N (**Fig.S7**). **Fig. 3a** illustrates the XPS spectra of the Ti 2p region. Ti 2p spectrum shows a binding energy at 459.4 eV and 465.1 eV for Ti $2p_{3/2}$ and Ti $2p_{1/2}$, respectively, corresponding to the Ti 2p spectrum from TiO_2. The signals of displayed peaks from C-C (288.3 eV), β-C (284.1 eV), α-C (285.0 eV) and other small peaks from C-N (286.0 eV), C-O (287.3 eV) and carbonates (289.4 eV) are corresponding to C 1s of PPy_{NS} (**Fig. 3b**). The signal at 400.0 eV was assigned to the –NH- group of the pyrrole unit, and the $-N^+-$ (polaron) and =N- defects of PPy structures are at 401.6 eV and 398.1 eV, respectively (**Fig. 3c**). The signals at 530.6 eV and 532.9 eV correspond to the O 1s of TiO_2 and SiO_2 (Si plate as a support) (**Fig. 3d**)[34]. All these results demonstrate that there is no new component produced in the composite PPy_{NS}-TiO_2, which is consistent with the XRD results (**Fig. 1d**).

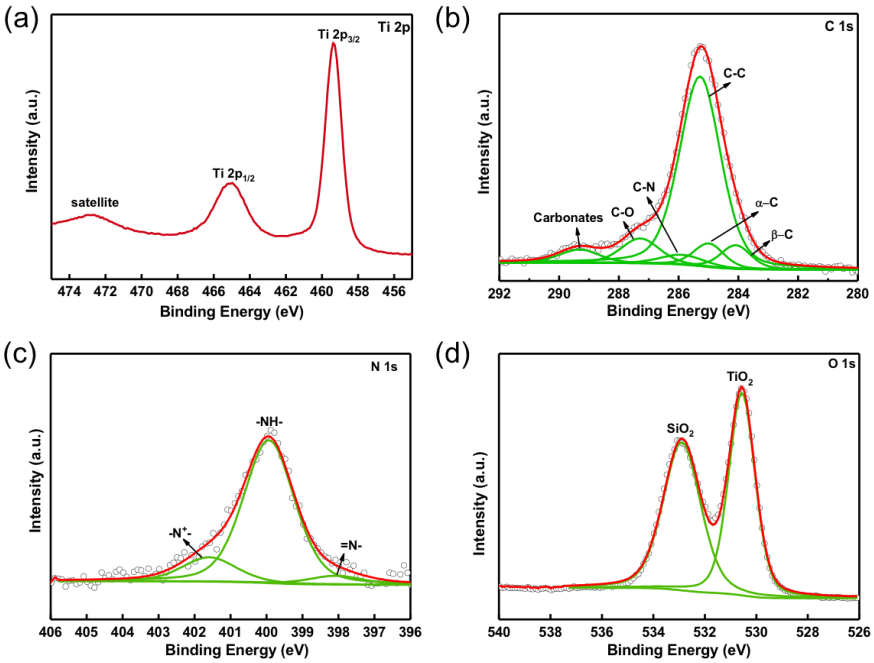

Fig.3. XPS spectra of PPy_{NS}-TiO_2 (a) Ti 2p of TiO_2, (b) C 1s of PPy_{NS}, (c) N 1s of PPy_{NS} and (d) O 1s of TiO_2 and SiO_2

TRMC technique was conducted to study the dynamics of charge carriers in the TiO_2-based composites [45]. The maximum data (I_{max}) provided by TRMC signals indicate the excess electrons number generated by the laser pulse and the decay of the signal is attributed to recombination and trapping processes representing the life-time of charge carriers. The samples were excited at different wavelengths under UV and visible light (360 nm, 420 nm, 450 nm, 500 nm).

As stated before, in TiO_2, electrons are much more mobile than holes, and the TRMC signals are largely corresponding to the e^- in the conduction band (CB). At 360 nm excitation (**Fig. 4a**), above TiO_2 bandgap, both bare TiO_2 and PPy_{NS}-TiO_2 present high I_{max} values. The signal of bare TiO_2 is higher than signal of the PPy_{NS}-TiO_2 composite, which indicates more charge carriers generated in pure TiO_2 under UV light. The decay is quite identical for both compounds. The lower signal decay in PPy_{NS}-TiO_2 may be due to PPy_{NS} shield effect, fast recombination effect, or fast electron trapping [46]. The similar decays show that no real important influence on charge carrier lifetime is detected.

However, under visible excitation, below TiO_2 bandgap, at 420 nm (**Fig. 4b**), 450 nm (**Fig. 4c**) and 500 nm (**Fig. 4d**), the signals of PPy_{NS}-TiO_2 increased relatively with the higher excitation wavelength, and the I_{max} signal of PPy_{NS}-TiO_2 is higher than that of TiO_2 at 450 nm and 500 nm excitation. The signal decay is also slower in the composite material, and this is related to longer life time of charge carriers due to less e^--h^+ recombination or rapid electron trapping. The signal intensity of PPy_{NS}-TiO_2 at 500 nm is slightly lower than that obtained with 450 nm excitation. These results demonstrate the formation of a heterojunction between PPy_{NS} and TiO_2, which induces electrons transfer from PPy_{NS} to TiO_2 under visible light and extension of the life time of charge carriers under UV and visible light.

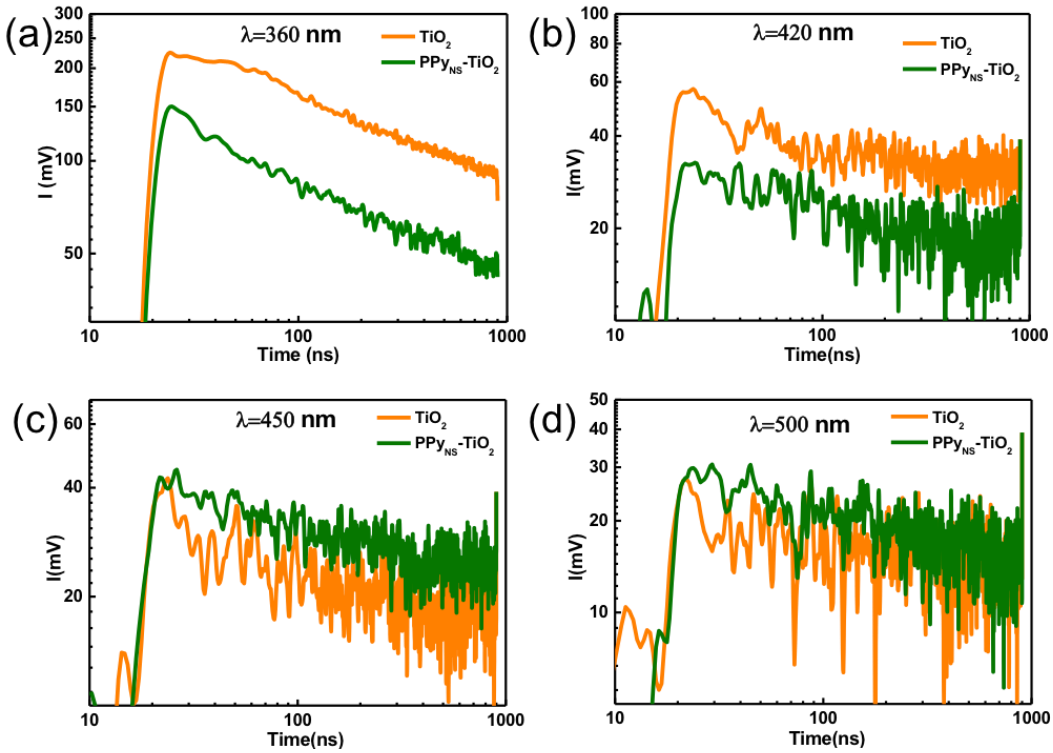

Fig. 4. TRMC signals of PPy_{NS}-TiO_2 and TiO_2 at different excitation wavelengths: (a) 360 nm UV irradiation, (b) 420 nm, (c) 450 nm, and (d) 500 nm visible irradiation. The corresponding laser energy was 0.9, 2.3, 2.3 and 2.3 $mJ \cdot cm^{-2}$, respectively.

Fig. 5a shows the photoinduced i-t curve of PPy_{NS}-TiO_2 and TiO_2 photoanodes under UV-vis light irradiation. The photocurrent of PPy_{NS}-TiO_2 photoanode was about 80 $\mu A \cdot cm^{-2}$, which is twice higher than that of TiO_2 photoanode, implying TiO_2 modification with PPy_{NS} increases generation, separation and transfer of charge carriers leading to the enhanced photoelectrochemical property [47]. EIS Nyquist plots showed that PPy_{NS}-TiO_2 exhibits a smaller semicircle compared to the TiO_2 (**Fig. 5b**), suggesting that PPy_{NS} may provide electron transfer channel for the PPy_{NS}-TiO_2/FTO photoanode, which increases the life time of electrons and ultimately enhances the photocatalytic activity [48, 49].

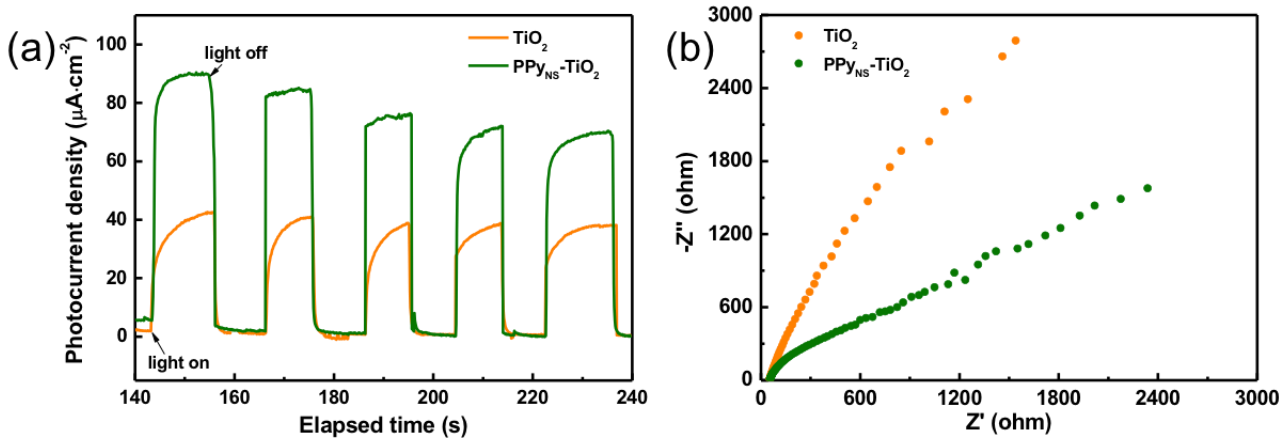

Fig. 5. (a) Photocurrent transient responses at a constant potential of -200 mV for TiO_2 and PPy_{NS}-TiO_2 FTO electrodes under UV-vis light irradiation; (b) the EIS curve of PPy_{NS}-TiO_2 and TiO_2 photoanodes under dark at the potential of 0.2 V vs Ag/AgCl in 0.1 M Na_2SO_4 neutral electrolyte.

3.2. Photocatalytic tests

The photocatalytic activity of the PPy_{NS}-TiO_2 composite was studied for degradation of model pollutants in water and in air.

MO and phenol were used as a water model pollutant. The effect of the mass ratios between PPy_{NS} and TiO_2 (PPy_{NS}: TiO_2 = 0:1, 1:2, 1:1, 2:1, 1:0) for photocatalytic degradation of MO was investigated and the best mass ratio with the highest photocatalytic activity is 1:1 (see in **Fig. S8**). **Fig. 6 and Fig. S9** shows the degradation of methyl orange and phenol in aqueous solution. Under UV-vis light, the effective degradation of MO up to 100% takes place in 20 min in the presence of PPy_{NS}-TiO_2 and PPy_{bulk}-TiO_2 composite, while this total degradation is achieved after 45 min irradiation with bare TiO_2 and with PPy_{NS} only 78% degradation is obtained after 5 h **(Fig. S10)**. The photocatalytic activity of PPy-TiO_2 is close to that of plasmonic TiO_2 (TiO_2 surface modified with Ag nanoparticles) as shown in **Fig. 6a** [12]. Bare TiO_2 is known to be not active under visible light irradiation. PPy_{NS}-TiO_2

composite shows a good photocatalytic activity: 70% of degradation rate of MO is achieved after 4 h under visible light. This activity is much higher than that of bare PPy_{NS} (18% degradation after 4 h) and also much higher than that of plasmonic TiO_2 (20% degradation after 5 h), and interestingly higher than that of PPy_{bulk}-TiO_2 (41% degradation after 4 h) (see in **Fig. 6b**)

These photocatalysts were also tested for phenol degradation. **Fig. 6c** shows that phenol is completely degraded in 20 min in the presence of PPy_{NS}-TiO_2, PPy_{bulk}-TiO_2, or 0.5%Ag-TiO_2 under UV-vis light. Besides, 100% degradation rate is achieved, respectively with bare TiO_2 after 25 min and with bare PPy_{NS} after 4.5 h. The activity of PPy_{bulk}-TiO_2 and plasmonic TiO_2 are very similar for phenol degradation under visible light. The photocatalytic activity of PPy_{NS}-TiO_2 is much higher than that of PPy_{bulk}-TiO_2, 0.5%Ag-TiO_2 and bare PPy_{NS} (no photocatalytic activity of bare TiO_2). The degradation rates of phenol are respectively: 55%, 25%, 15% and 10% with PPy_{NS}-TiO_2, PPy_{bulk}-TiO_2, 0.5%Ag-TiO_2 and bare PPy_{NS} after 4 h irradiation under visible light (**Fig. 6d, and Fig. S11** and **Fig. S12**). TOC (total organic carbon) measurements indicate the decontamination level of water. 91% of phenol were mineralized after 20 min of UV irradiation in the presence of PPy_{NS}-TiO_2. Table S1 shows some photocatalytic results for water treatment reported for other composite materials based on TiO_2 and conjugated polymers for comparison with the present work: Our photocatalyst (PPy_{NS}-TiO_2) shows a higher photocatalytic activity under visible light. Note that the comparison is a rough assessment due to the different experimental conditions such as light source, catalysts quality, pollutant type etc.

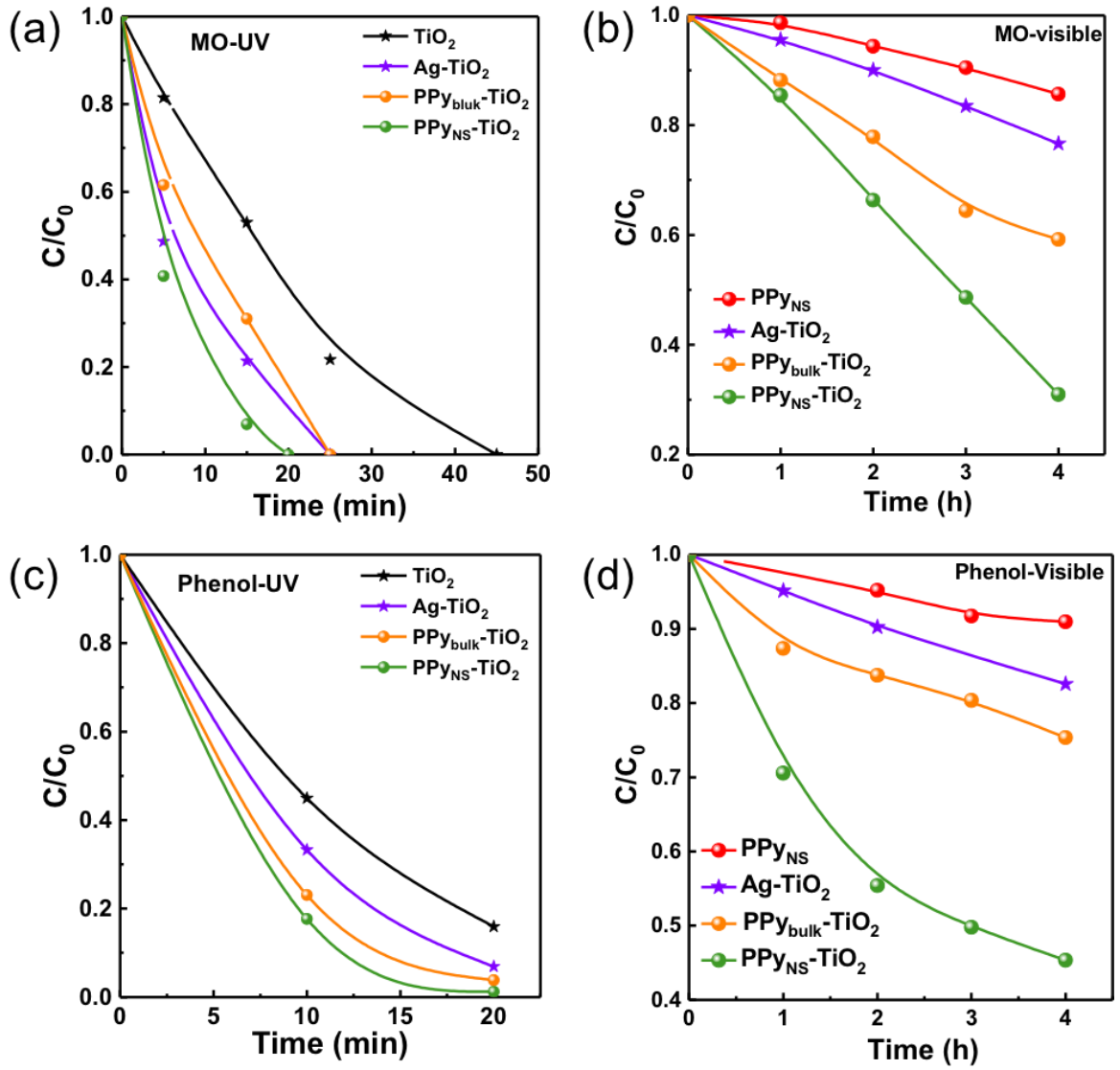

Fig. 6. Photocatalytic degradation rate of MO (C_0 = 500 ppm) in the presence of as-prepared samples under UV (a) and visible light irradiation (b); photocatalytic degradation rate of phenol under UV (c) and visible light irradiation (d).

The photocatalytic activity for air treatment of PPy_{NS} and PPy_{NS}-TiO_2 composite was evaluated, and toluene was taken as model pollutant. **Fig 7** shows toluene degradation at different irradiation wavelength (375 nm, 415 nm and 465 nm). Under UV irradiation (λ = 375 nm), TiO_2 shows the best

photocatalytic activity compared to PPy_{NS} and PPy_{NS}-TiO_2: After 50 min irradiation, the degradation rate with TiO_2 is 100%, while with PPy_{NS} and PPy_{NS}-TiO_2 it is, 49% and 92% respectively. The photodegradation rate of PPy_{NS}-TiO_2 is twice higher than that of pure PPy_{NS} under UV light (**Fig. 7a**). More importantly, under visible light (λ = 415 and 465 nm), PPy_{NS}-TiO_2 shows better photocatalytic performance than PPy_{NS} (TiO_2 presents no photocatalytic activity under visible light). The degradation rates of PPy_{NS}-TiO_2 are 80% (λ = 415 nm) and 55% (λ = 465 nm) after 100 min, respectively, which are much higher than that obtained with PPy_{NS} (45% under λ = 415 nm and 33% under λ = 465 nm irradiation) (**Fig. 7b-c**).

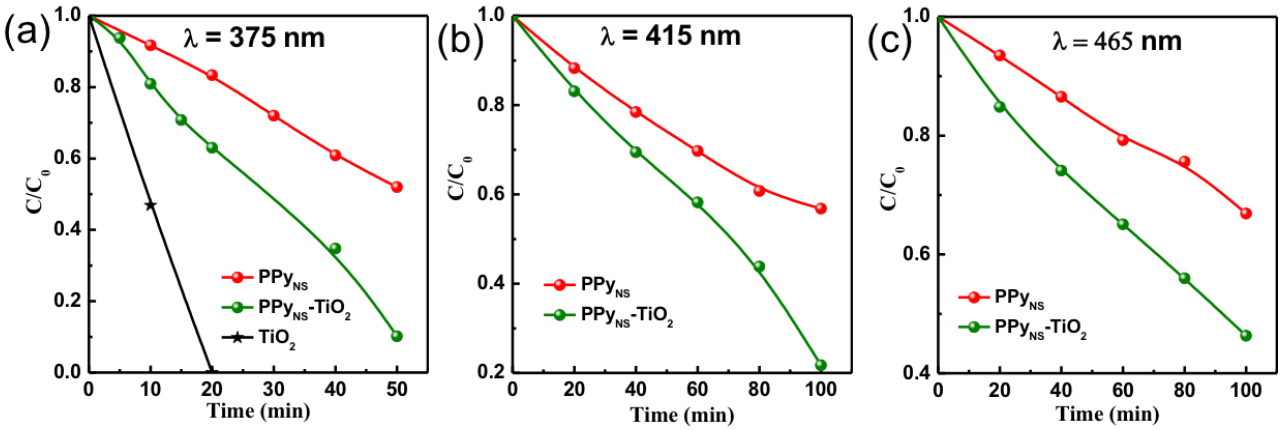

Fig. 7. Photocatalytic activity of PPy_{NS} and PPy_{NS}-TiO_2 for the toluene degradation under (a) λ = 375 nm, (b) 415 nm, and (c) 465 nm irradiation, respectively.

The results show that PPy_{NS}-TiO_2 composites are very efficient for MO, phenol and toluene degradation under visible light irradiation. The formation of a p-n heterojunction between PPy nanostructures and TiO_2 decreased the recombination of photogenerated charge-carriers and enhanced the photocatalytic performance of the composite PPy_{NS}-TiO_2.

In order to satisfy the practical application, the stability and reusability of the photocatalyst was investigated. The photocatalytic activity of PPy_{NS}-TiO_2 is stable after 6 cycles as shown in **Fig. S13 Fig. S14**. These results indicate that PPy_{NS}-TiO_2 is a very promising photocatalyst for water and air treatment and other photocatalytic applications.

3.3. Photocatalytic mechanism

A huge number of defects could be accumulated at the contact interface of various solids and the energy levels of the interface are quasi-continuous, exhibiting alike properties to conductors. This contact interface can also produce low electric resistance Ohmic contacts and serve as the center of charge carriers' recombination [50].

CPs behave as classical organic semiconductors. The nanostructutration of a conjugated polymer is a pivotal factor for its photocatalytic activity. The morphology and size of the photocatalytic nanomaterials have an important effect on their photocatalytic performance, as demonstrated for TiO_2 for example [51, 52] or for CP nanostructures [31-33]. The difference in the photocatalytic property between nano and bulk CPs may be owing to larger sizes, larger surface areas, and more defects in bulk CPs, which are responsible for the e^--h^+ recombinations [31, 32].

Under UV irradiation, the photoinduced e^- in the CB of TiO_2 can recombine with the h^+ in the highest occupied orbital (HOMO) of PPy_{NS} via the intimate interface resulting the separation of photogenerated charge carriers (see **Fig. 8a**), which explains the decreased intensity signal of PPy_{NS}-TiO_2 in TRMC measurement at the excitation of 365 nm and 400 nm wavelength compared with bare TiO_2. In this case, the oxidative reaction and reductive species are produced in the VB band of TiO_2

($h^+ + OH^- \rightarrow {}^{\bullet}OH$, +2.7 V vs. NHE at pH = 0) and the lowest unoccupied orbital (LUMO) of PPy_{NS} ($e^- + O_2 \rightarrow O_2^{\bullet-}$, -0.046 V vs. NHE at pH = 0), respectively [53]. This proposed mechanism is highly in agreement with the results of TRMC and photocatalytic properties under UV irradiation.

However, the higher yield and longer life time of charge carriers from the TRMC measurements and higher photocatalytic activity in the presence of PPy_{NS}-TiO_2 composite compared to pristine TiO_2 under visible light excitation, another possible photocatalytic mechanism can be proposed for PPy_{NS}-TiO_2 (see **Fig. 8b**). Under visible light irradiation, only PPy_{NS} can be photoexcited and act as a photosensitizer. Owing to the internal electric field function, the e^- in the LUMO of PPy_{NS} could be transferred to that of CB of TiO_2. Photogenerated h^+ located on the HOMO of PPy_{NS} can participate in the oxidative reaction [54]. As a result, the redox reaction happens in the CB of TiO_2 (reductive reaction: $A \rightarrow A^-$) and HOMO of PPy_{NS} (oxidative reaction: $D \rightarrow D^+$), and the effective charge separation can extend the life time of generated e^- and h^+ and then enhance photocatalytic activity.

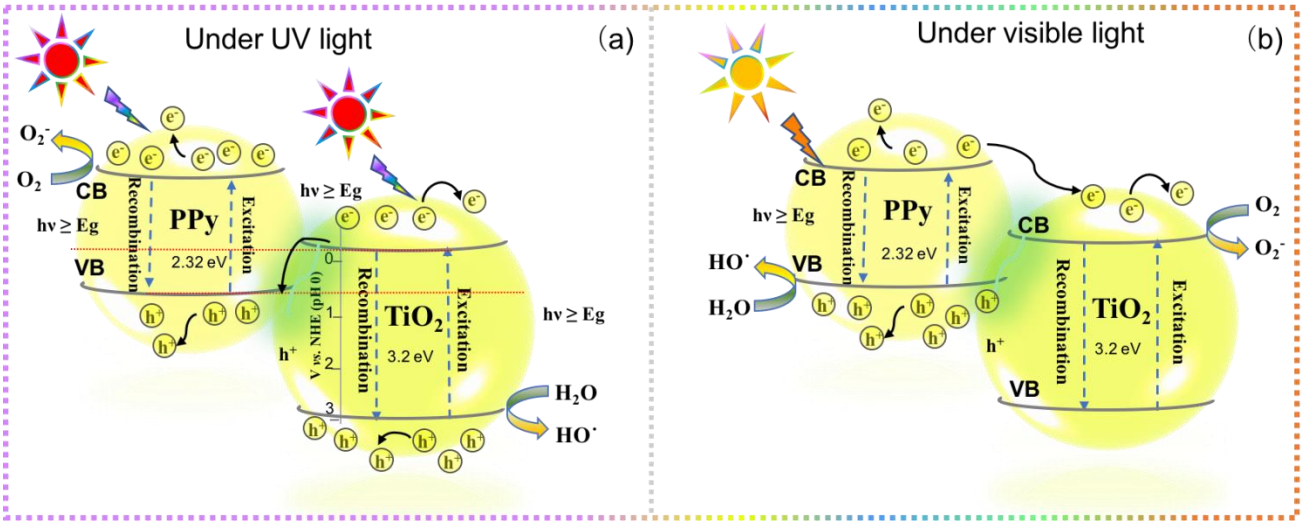

Fig. 8. Proposed photocatalytic mechanism for the PPy_{NS}-TiO_2 system and charge transfer mechanisms under UV light (a), and under visible light irradiation (b).

4. Conclusions

We have prepared a highly photoactive PPy_{NS}-TiO_2 nanocomposite under visible for environmental pollution remediation. PPy_{NS}-TiO_2 presents a red-shift of the absorption band edge and a significant reduction of the band gap (1.95 eV). Our experiments demonstrate that for water and air treatment PPy nanostructures modified with TiO_2 exhibit under visible light higher photocatalytic activity than plasmonic TiO_2, PPy_{NS} and PPy_{bulk}-TiO_2 . This enhancement of the photocatalytic activity is due to the nanostructuration of the CP and the heterojunction formation at the interface between PPy_{NS} and TiO_2, which promotes the seperation of photoinduced e^- and h^+.

Interstingly, the composite PPy_{NS}-TiO_2 has much higher photocatalytic performance than PPy_{bulk}-TiO_2 : Indeed, conjugated polymers nanostructuration is a pivotal factor for photocatalytic applications. Highest surface area and less number of defects in nanostructured polymers (which induce less electron-hole recombinations), lead to higher photocatalytic activity compared to their bulk conterparts [31-33]. The photocatalytic activity is stable with cycling.

This work provides a facile way to develop cheap and very active organic-inorganic hybrid nanocomposite materials for air and water treatment. This stable nanocomposite can also find applications in self cleaning surfaces. Future works will also focus on its modification with cocatalysts based on abondant elements for water splitting.

Acknowledgements

X.Y. gratefully acknowledges the financial support from China Scholarship Council (CSC). This work was supported by the IDEX Paris-Saclay and IRS MOMENTOM.

Reference

[1] K. Nakata, A. Fujishima, TiO_2 photocatalysis: Design and applications, Journal of Photochemistry and Photobiology C: Photochemistry Reviews, 13 (2012) 169-189. https://doi.org/10.1016/j.jphotochemrev.2012.06.001.

[2] K. Hashimoto, H. Irie, A. Fujishima, TiO_2 photocatalysis: a historical overview and future prospects, Japanese Journal of Applied Physics, 44 (2005) 8269-8285. https://iopscience.iop.org/article/10.1143/JJAP.44.8269/meta.

[3] L. Yang, E.Y. Liya, M.B. Ray, Degradation of paracetamol in aqueous solutions by TiO_2 photocatalysis, Water Research, 42 (2008) 3480-3488. https://doi.org/10.1016/j.watres.2008.04.023.

[4] D. Sánchez-Rodríguez, M.G.M. Medrano, H. Remita, V. Escobar-Barrios, Photocatalytic properties of BiOCl-TiO_2 composites for phenol photodegradation, Journal of Environmental Chemical Engineering, 6 (2018) 1601-1612. https://doi.org/10.1016/j.jece.2018.01.061.

[5] M.G. Méndez-Medrano, E. Kowalska, M. Endo-Kimura, K. Wang, B. Ohtani, D. Bahena Uribe, J.L. Rodríguez-López, H. Remita, Inhibition of Fungal Growth Using Modified TiO_2 with Core@ Shell Structure of Ag@ CuO Clusters, ACS Applied Bio Materials, 2(2019) 5626-5633. https://doi.org/10.1021/acsabm.9b00707.

[6] H. Kaur, S. Kumar, N. Verma, P. Singh, Role of pH on the photocatalytic activity of TiO_2 tailored by W/T mole ratio, Journal of Materials Science: Materials in Electronics, 29 (2018) 16120-16135. https://doi.org/10.1007/s10854-018-9701-0.

[7] Y. Choi, M.S. Koo, A.D. Bokare, D.-h. Kim, D.W. Bahnemann, W. Choi, Sequential process combination of photocatalytic oxidation and dark reduction for the removal of organic pollutants and Cr (VI) using Ag/TiO_2, Environmental Science & Technology, 51 (2017) 3973-3981. https://doi.org/10.1021/acs.est.6b06303.

[8] V. Vaiano, G. Iervolino, D. Sannino, J.J. Murcia, M.C. Hidalgo, P. Ciambelli, J.A. Navío, Photocatalytic removal of patent blue V dye on Au-TiO_2 and Pt-TiO_2 catalysts, Applied Catalysis B: Environmental, 188 (2016) 134-146. https://doi.org/10.1016/j.apcatb.2016.02.001.

[9] E. Kowalska, H. Remita, C. Colbeau-Justin, J. Hupka, J. Belloni, Modification of titanium dioxide with platinum ions and clusters: application in photocatalysis, The Journal of Physical Chemistry C, 112 (2008) 1124-1131. https://doi.org/10.1021/jp077466p.

[10] E. Grabowska, A. Zaleska, S. Sorgues, M. Kunst, A. Etcheberry, C. Colbeau-Justin, H. Remita, Modification of titanium (IV) dioxide with small silver nanoparticles: application in photocatalysis, The Journal of Physical Chemistry C, 117 (2013) 1955-1962. https://doi.org/10.1021/jp3112183.

[11] Z. Hai, N. El Kolli, D.B. Uribe, P. Beaunier, M. José-Yacaman, J. Vigneron, A. Etcheberry, S. Sorgues, C. Colbeau-Justin, J. Chen, Modification of TiO_2 by bimetallic Au–Cu nanoparticles for wastewater treatment, Journal of Materials Chemistry A, 1 (2013) 10829-10835. https://doi.org/10.1039/C3TA11684K.

[12] M. Méndez-Medrano, E. Kowalska, A. Lehoux, A. Herissan, B. Ohtani, D. Bahena, V. Briois, C. Colbeau-Justin, J. Rodríguez-López, H. Remita, Surface modification of TiO_2 with Ag nanoparticles and CuO nanoclusters for application in photocatalysis, The Journal of Physical Chemistry C, 120 (2016) 5143-5154. https://doi.org/10.1021/acs.jpcc.5b10703.

[13] M. Méndez-Medrano, E. Kowalska, A. Lehoux, A. Herissan, B. Ohtani, S. Rau, C. Colbeau-Justin, J. Rodríguez-López, H. Remita, Surface modification of TiO_2 with Au nanoclusters for efficient water treatment and hydrogen generation under visible light, The Journal of Physical Chemistry C, 120 (2016) 25010-25022. https://doi.org/10.1021/acs.jpcc.6b06854.

[14] Y. Zhang, Z. Zhao, J. Chen, L. Cheng, J. Chang, W. Sheng, C. Hu, S. Cao, C-doped hollow TiO_2 spheres: in situ synthesis, controlled shell thickness, and superior visible-light photocatalytic activity, Applied Catalysis B: Environmental, 165 (2015) 715-722. https://doi.org/10.1016/j.apcatb.2014.10.063.

[15] J. Shao, W. Sheng, M. Wang, S. Li, J. Chen, Y. Zhang, S. Cao, In situ synthesis of carbon-doped TiO_2 single-crystal nanorods with a remarkably photocatalytic efficiency, Applied Catalysis B: Environmental, 209 (2017) 311-319. https://doi.org/10.1016/j.apcatb.2017.03.008.

[16] T.M. Khedr, S.M. El-Sheikh, A. Hakki, A.A. Ismail, W.A. Badawy, D.W. Bahnemann, Highly active non-metals doped mixed-phase TiO_2 for photocatalytic oxidation of ibuprofen under visible light, Journal of Photochemistry and Photobiology A: Chemistry, 346 (2017) 530-540. https://doi.org/10.1016/j.jphotochem.2017.07.004.

[17] Y. Xia, Q. Li, K. Lv, M. Li, Heterojunction construction between TiO_2 hollowsphere and $ZnIn_2S_4$ flower for photocatalysis application, Applied Surface Science, 398 (2017) 81-88. https://doi.org/10.1016/j.apsusc.2016.12.006.

[18] X.-j. Wang, W.-y. Yang, F.-t. Li, J. Zhao, R.-h. Liu, S.-j. Liu, B. Li, Construction of amorphous TiO_2/BiOBr heterojunctions via facets coupling for enhanced photocatalytic activity, Journal of Hazardous Materials, 292 (2015) 126-136. https://doi.org/10.1016/j.jhazmat.2015.03.030.

[19] P. Zhang, L. Yu, X.W. Lou, Construction of Heterostructured Fe_2O_3-TiO_2 Microdumbbells for Photoelectrochemical Water Oxidation, Angewandte Chemie, 130 (2018) 15296-15300. https://doi.org/10.1002/anie.201808104.

[20] L. Yang, Y. Yu, J. Zhang, F. Chen, X. Meng, Y. Qiu, Y. Dan, L. Jiang, In-situ fabrication of diketopyrrolopyrrole-carbazole-based conjugated polymer/TiO_2 heterojunction for enhanced visible light photocatalysis, Applied Surface Science, 434 (2018) 796-805. https://doi.org/10.1016/j.apsusc.2017.10.176.

[21] Y. Wen, S. Liu, Q. Zhang, Y. Zhang, Z. Yang, A. Zhu, Partially conjugated polyvinyl chloride-modified TiO_2 nanoparticles for efficient visible-light-driven photocatalytic reduction of aqueous Cr (VI), Materials Letters, 163 (2016) 262-265. https://doi.org/10.1016/j.matlet.2015.10.109.

[22] F. Gao, X. Hou, A. Wang, G. Chu, W. Wu, J. Chen, H. Zou, Preparation of polypyrrole/TiO_2 nanocomposites with enhanced photocatalytic performance, Particuology, 26 (2016) 73-78. https://doi.org/10.1016/j.partic.2015.07.003.

[23] E.R. Macedo, P.S. Oliveira, H.P. de Oliveira, Synthesis and characterization of branched polypyrrole/titanium dioxide photocatalysts, Journal of Photochemistry and Photobiology A: Chemistry, 307 (2015) 108-114. https://doi.org/10.1016/j.jphotochem.2015.04.013.

[24] J. Zhang, H. Yang, S. Xu, L. Yang, Y. Song, L. Jiang, Y. Dan, Dramatic enhancement of visible light photocatalysis due to strong interaction between TiO_2 and end-group functionalized P3HT, Applied Catalysis B: Environmental, 174 (2015) 193-202. https://doi.org/10.1016/j.apcatb.2015.02.034.

[25] Y. Song, F. Massuyeau, L. Jiang, Y. Dan, P. Le Rendu, T. Nguyen, Effect of graphene size on the photocatalytic activity of TiO_2/poly (3-hexylthiophene)/graphene composite films, Catalysis Today, 321 (2019) 74-80. https://doi.org/10.1016/j.cattod.2018.04.045.

[26] S. Sardar, P. Kar, H. Remita, B. Liu, P. Lemmens, S.K. Pal, S. Ghosh, Enhanced charge separation and FRET at heterojunctions between semiconductor nanoparticles and conducting polymer nanofibers for efficient solar light harvesting, Scientific Reports, 5 (2015) 17313. https://doi.org/10.1038/srep17313.

[27] N.M. Dimitrijevic, S. Tepavcevic, Y. Liu, T. Rajh, S.C. Silver, D.M. Tiede, Nanostructured TiO_2/polypyrrole for visible light photocatalysis, The Journal of Physical Chemistry C, 117 (2013) 15540-15544. https://doi.org/10.1021/jp405562b.

[28] G. Mamba, A. Mishra, Graphitic carbon nitride (g-C_3N_4) nanocomposites: a new and exciting generation of visible light driven photocatalysts for environmental pollution remediation, Applied Catalysis B: Environmental, 198 (2016) 347-377. https://doi.org/10.1016/j.apcatb.2016.05.052.

[29] S. Ghosh, H. Remita, R.N. Basu, Visible-light-induced reduction of Cr (VI) by PDPB-ZnO nanohybrids and its photo-electrochemical response, Applied Catalysis B: Environmental, 239 (2018)

362-372. https://doi.org/10.1016/j.apcatb.2018.08.034.

[30] S. Ghosh, L. Ramos, H. Remita, Swollen hexagonal liquid crystals as smart nanoreactors: implementation in materials chemistry for energy applications, Nanoscale, 10 (2018) 5793-5819. https://doi.org/10.1039/C7NR08457A.

[31] X. Yuan, D. Floresyona, P.-H. Aubert, T.-T. Bui, S. Remita, S. Ghosh, F. Brisset, F. Goubard, H. Remita, Photocatalytic degradation of organic pollutant with polypyrrole nanostructures under UV and visible light, Applied Catalysis B: Environmental, 242 (2019) 284-292. https://doi.org/10.1016/j.apcatb.2018.10.002.

[32] D. Floresyona, F. Goubard, P.-H. Aubert, I. Lampre, J. Mathurin, A. Dazzi, S. Ghosh, P. Beaunier, F. Brisset, S. Remita, L. Ramos, R. Hynd, Highly active poly (3-hexylthiophene) nanostructures for photocatalysis under solar light, Applied Catalysis B: Environmental, 209 (2017) 23-32. https://doi.org/10.1016/j.apcatb.2017.02.069.

[33] S. Ghosh, N.A. Kouamé, L. Ramos, S. Remita, A. Dazzi, A. Deniset-Besseau, P. Beaunier, F. Goubard, P.-H. Aubert, H. Remita, Conducting polymer nanostructures for photocatalysis under visible light, Nature Materials, 14 (2015) 505-511. https://doi.org/10.1038/nmat4220.

[34] Q. Luo, X. Li, D. Wang, Y. Wang, J. An, Photocatalytic activity of polypyrrole/TiO_2 nanocomposites under visible and UV light, Journal of Materials Science, 46 (2011) 1646-1654. https://doi.org/10.1007/s10853-010-4981-7.

[35] S. Ghosh, N.A. Kouame, S. Remita, L. Ramos, F. Goubard, P.-H. Aubert, A. Dazzi, A. Deniset-Besseau, H. Remita, Visible-light active conducting polymer nanostructures with superior photocatalytic activity, Scientific reports, 5 (2015) 1-9. https://doi.org/10.1038/srep18002.

[36] S. Ghosh, L. Ramos, S. Remita, A. Dazzi, A. Deniset-Besseau, P. Beaunier, F. Goubard, P.-H. Aubert, H. Remita, Conducting polymer nanofibers with controlled diameters synthesized in hexagonal mesophases, New Journal of Chemistry, 39 (2015) 8311-8320. https://doi.org/10.1039/C5NJ00826C.

[37] S. Ghosh, H. Remita, L. Ramos, A. Dazzi, A. Deniset-Besseau, P. Beaunier, F. Goubard, P.-H. Aubert, F. Brisset, S. Remita, PEDOT nanostructures synthesized in hexagonal mesophases, New Journal of Chemistry, 38 (2014) 1106-1115. https://doi.org/10.1039/C3NJ01349A.

[38] W. is Degussa, P25? Crystalline composition analysis, reconstruction from isolated pure particles and photocatalytic activity test, Ohtani B., Prieto-Mahaney OO, Abe R, Journal of Photochemistry and Photobiology A: Chemistry, 216 (2010) 179-182. https://doi.org/10.1016/j.jphotochem.2010.07.024.

[39] N. Serpone, G. Sauve, R. Koch, H. Tahiri, P. Pichat, P. Piccinini, E. Pelizzetti, H. Hidaka,

Standardization protocol of process efficiencies and activation parameters in heterogeneous photocatalysis: relative photonic efficiencies ζr, Journal of Photochemistry and Photobiology A: Chemistry, 94 (1996) 191-203. https://doi.org/10.1016/1010-6030(95)04223-7.

[40] A. Sobczyński, Ł. Duczmal, W. Zmudziński, Phenol destruction by photocatalysis on TiO_2: an attempt to solve the reaction mechanism, Journal of Molecular Catalysis A: Chemical, 213 (2004) 225-230. https://doi.org/10.1016/j.molcata.2003.12.006.

[41] U. Baig, M. Gondal, A. Ilyas, M. Sanagi, Band gap engineered polymeric-inorganic nanocomposite catalysts: Synthesis, isothermal stability, photocatalytic activity and photovoltaic performance, Journal of Materials Science & Technology, 33 (2017) 547-557. https://doi.org/10.1016/j.jmst.2016.11.031.

[42] Y. Zhao, W. Zhu, G.Z. Chen, E.J. Cairns, Polypyrrole/TiO_2 nanotube arrays with coaxial heterogeneous structure as sulfur hosts for lithium sulfur batteries, Journal of Power Sources, 327 (2016) 447-456. https://doi.org/10.1016/j.jpowsour.2016.07.082.

[43] S. Cui, L. Yang, J. Wang, X. Wang, Fabrication of a sensitive gas sensor based on PPy/TiO_2 nanocomposites films by layer-by-layer self-assembly and its application in food storage, Sensors and Actuators B: Chemical, 233 (2016) 337-346. https://doi.org/10.1016/j.snb.2016.04.093.

[44] S. Cao, H. Zhang, Y. Song, J. Zhang, H. Yang, L. Jiang, Y. Dan, Investigation of polypyrrole/polyvinyl alcohol–titanium dioxide composite films for photo-catalytic applications, Applied Surface Science, 342 (2015) 55-63. https://doi.org/10.1016/j.apsusc.2015.02.139.

[45] H. Remita, M.G. Méndez Medrano, C. Colbeau-Justin, Effect of Modification of TiO_2 with Metal Nanoparticles on Its Photocatalytic Properties Studied by Time-Resolved Microwave Conductivity, Visible Light-Active Photocatalysis: Nanostructured Catalyst Design, Mechanisms, and Applications, (2018) 129-164.

[46] C.A. Emilio, M.I. Litter, M. Kunst, M. Bouchard, C. Colbeau-Justin, Phenol photodegradation on platinized-TiO_2 photocatalysts related to charge-carrier dynamics, Langmuir, 22 (2006) 3606-3613. https://doi.org/10.1021/la051962s.

[47] F. Deng, L. Min, X. Luo, S. Wu, S. Luo, Visible-light photocatalytic degradation performances and thermal stability due to the synergetic effect of TiO_2 with conductive copolymers of polyaniline and polypyrrole, Nanoscale, 5 (2013) 8703-8710. https://doi.org/10.1039/C3NR02502K.

[48] J. Li, X. Gao, X. Jiang, X.-B. Li, Z. Liu, J. Zhang, C.-H. Tung, L.-Z. Wu, Graphdiyne: A Promising Catalyst–Support To Stabilize Cobalt Nanoparticles for Oxygen Evolution, ACS Catalysis, 7 (2017) 5209-5213. https://doi.org/10.1021/acscatal.7b01781.

[49] J. Li, X. Gao, Z. Li, J.H. Wang, L. Zhu, C. Yin, Y. Wang, X.B. Li, Z. Liu, J. Zhang, Superhydrophilic Graphdiyne Accelerates Interfacial Mass/Electron Transportation to Boost Electrocatalytic and Photoelectrocatalytic Water Oxidation Activity, Advanced Functional Materials, 29 (2019) 1808079. https://doi.org/10.1002/adfm.201808079.

[50] J. Schneider, D. Bahnemann, J. Ye, G.L. Puma, D.D. Dionysiou, Photocatalysis: fundamentals and perspectives, Royal Society of Chemistry, 2016.

[51] B. Ohtani, O.O.P. Mahaney, F. Amano, N. Murakami, R. Abe, What are titania photocatalysts?—an exploratory correlation of photocatalytic activity with structural and physical properties, Journal of Advanced Oxidation Technologies, 13 (2010) 247-261. https://doi.org/10.1515/jaots-2010-0303.

[52] O.-O. Prieto-Mahaney, N. Murakami, R. Abe, B. Ohtani, Correlation between photocatalytic activities and structural and physical properties of titanium (IV) oxide powders, Chemistry Letters, 38 (2009) 238-239. https://doi.org/10.1246/cl.2009.238.

[53] Y. Bai, P.-Q. Wang, J.-Y. Liu, X.-J. Liu, Enhanced photocatalytic performance of direct Z-scheme BiOCl–g-C_3N_4 photocatalysts, RSC Advances, 4 (2014) 19456-19461. https://doi.org/10.1039/C4RA01629G.

[54] X. Li, P. Wang, B. Huang, X. Qin, X. Zhang, Q. Zhang, X. Zhu, Y. Dai, Precisely locate Pd-Polypyrrole on TiO_2 for enhanced hydrogen production, International Journal of Hydrogen Energy, 42 (2017) 25195-25202. https://doi.org/10.1016/j.ijhydene.2017.08.153.